



Synthesis and characterization of CoFe_2O_4 and Ni-doped CoFe_2O_4 nanoparticles by chemical Co-precipitation technique for photo-degradation of organic dyestuffs under direct sunlight

J. Revathi^a, M. John Abel^b, V. Archana^b, T. Sumithra^b, R. Thiruneelakandan^{c,*},
J. Joseph prince^{b,*}

^a Department of Physics, St. Antony's College of Arts and Sciences for Women, Ammakulathupatti, Tamil Nadu, 624005, India

^b Department of Physics, University College of Engineering, Bharathidasan Institute of Technology Campus, Anna University, Tiruchirappalli, 24, Tamil Nadu, India

^c Department of Chemistry, University College of Engineering, Bharathidasan Institute of Technology Campus, Anna University, Tiruchirappalli, 24, Tamil Nadu, India

ARTICLE INFO

Keywords:

Spinel ferrites
Photocatalytic activity
Sunlight irradiation
Optical properties
Nanoparticles

ABSTRACT

Cobalt ferrite and nickel doped cobalt ferrite nanoparticles (NPs) was victoriously developed through chemical co-precipitation technique. The spinel crystal structure of prepared samples was confirmed by powder X-ray diffraction studies (PXRD) and also the crystalline size was calculated. Optical properties of the samples were analyzed using UV–Visible spectrophotometer and Photoluminescence (PL) studies. The bandgap was calculated using Tauc's plot and is found to be 1.83 eV, 1.92 eV, 2.12 eV, and 2.21 eV for pure cobalt ferrite and (3, 7, 11) wt % Ni-doped CoFe_2O_4 samples respectively. Further, the morphological and the compositional weight percentage (wt %) was examined using a Scanning Electron Microscope (SEM) and Energy Dispersive X-ray spectrum (EDAX) respectively. Towards application, the photocatalytic activity of the synthesized NPs was studied under direct sunlight and the maximum efficiency was obtained as 83.41%, 63.62% and 82.76% for Methylene Blue (MB), Rhodamine B (RhB) and Crystal Violet (CV) respectively.

1. Introduction

The evolution of human societies led to the growth of huge industrialization. The cause of the growing urbanization and industrialization, our environment is facing the constant pressure of various environmental problems. Out of these, the world's top-most environmental problem is the purification of water. Consequently, the major thing that will be contaminating the natural water resources is the industries that utilizing or producing toxic organic pollutants such as fertilizers, chlorinated solvents, volatile organic compounds (VOCs), nitroaromatic compounds, phenols and dyes [1]. Among these, the organic dyes were vastly used in the textile industries, jute and threads industries, pharmaceutical industries, petrochemicals, etc. are released as effluent into the water resources like ponds, lakes, rivers and so on. These organic dyes and their products are generally toxic and may cause severe mutagenic effects, and carcinogenic effects in the vicinity of the biosphere [2]. The effective elimination of these toxic pollutants or the conversion of their toxic nature into some non-toxic and eco-friendly

products is of greatest practical importance. Thus, many efforts have been taken to remove those organic contaminants from the water. For instance, precipitation, ion exchange, flocculation and coagulation, electrochemical, biological methods, and membrane filtration are some of the conventional treatments for water purification [3,4]. In the evolution of wastewater treatment, now advanced oxidation processes (AOP) have emerged as the easiest and eco-friendly technology for the photocatalytic degradation of organic contaminants in wastewater [5–7].

In recent decades, emerging research attempts have been vastly focused on the synthesis of photocatalysts for the treatment of wastewaters with dangerous contaminants. For instance, there are variety of such catalysts have been synthesized alike, BN nanofibers [8], zeolites [9], rare-earth metal nanoparticles such as Palladium, silver, platinum, gold, [10–14], ferrites [15], composite materials [16,17], and metal oxides [18], which are very powerful for the degradation of such contaminants. Among these, the spinel ferrites have more attention because of their various properties like chemically stable, cost-effective, easy to

* Corresponding author.

** Corresponding author.

E-mail addresses: rtkchemaut@gmail.com (R. Thiruneelakandan), josephprinceaut@gmail.com (J. Joseph prince).

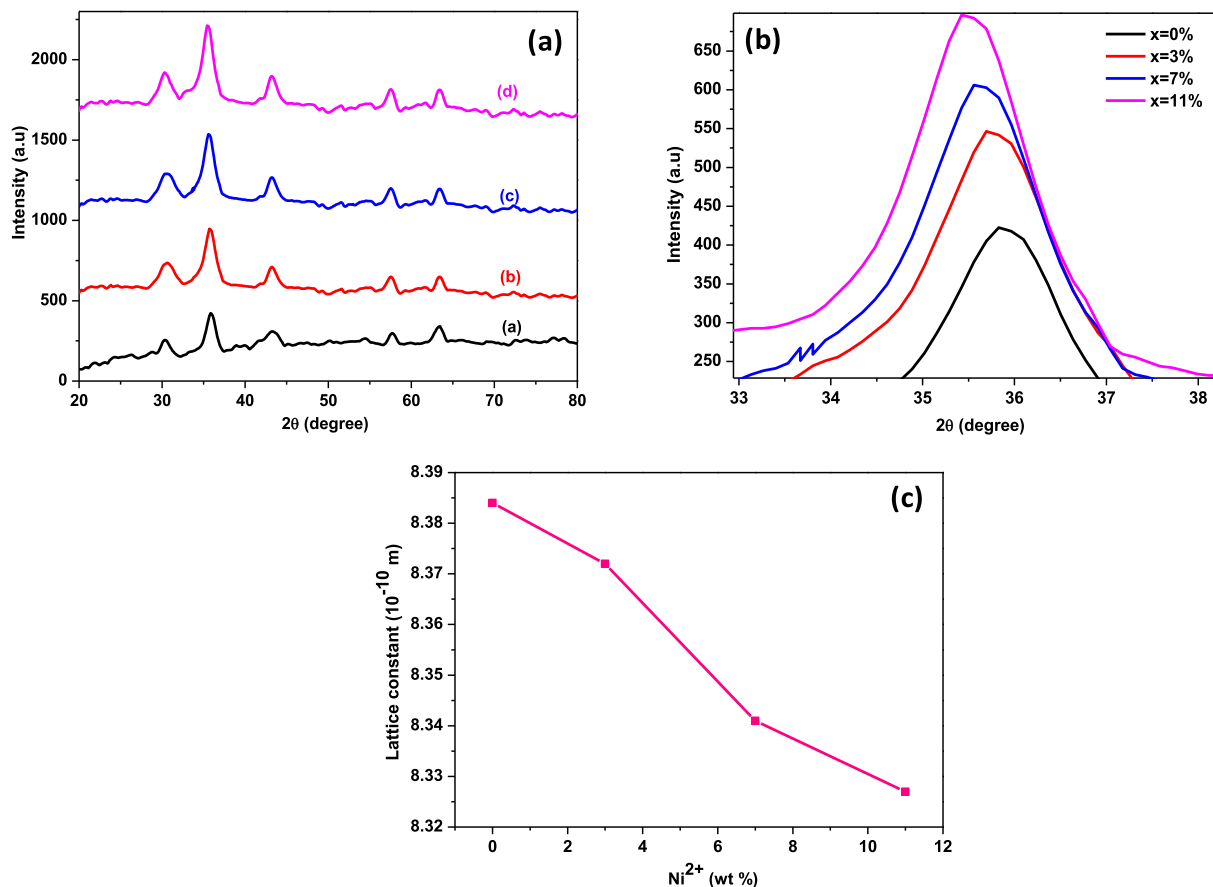


Fig. 1. (a & b) The powder X-ray diffraction pattern of CoFe₂O₄ and Ni-doped CoFe₂O₄ NPs (c) graph between Ni wt % and lattice constant.

Table 1

XRD comparison table of CoFe₂O₄ and Ni-doped CoFe₂O₄ NPs.

Samples	Peak position (2θ)	Lattice parameter (Å)	Particle size (nm)
CoFe ₂ O ₄	35.85	8.3846	40.23
Ni _{3%} Co _(100-3%) Fe ₂ O ₄	35.72	8.3685	41.56
Ni _{7%} Co _(100-7%) Fe ₂ O ₄	35.64	8.3421	42.38
Ni _{11%} Co _(100-11%) Fe ₂ O ₄	35.56	8.3276	43.15

synthesis, etc. Hence, many researchers have implant spinel ferrites for photocatalytic activity. A. I Borhan et al. has reported the photocatalytic activity of Aluminium doped Zinc Ferrite on Orange I dye [19]. The

photocatalytic activity of Ce doped Copper Ferrite on Methyl orange was reported by M. Rahimi-Nasrabadi et al. [20]. The photodegradation of Remazol Black 5 (RB5) with CuFe₂O₄, CoFe₂O₄, NiFe₂O₄, and ZnFe₂O₄, a comparative study were reported by R. Sharma et al. [21]. Indigo carmine (IC) dye was degraded using Mn-doped NiFe₂O₄ was reported by K. S. Jesudoss et al. [22]. CoFe₂O₄ is one of the indispensable spinel ferrites owing to their exclusive utilization in diverse fields like anti-bacterial [23], electrical [24], cancer treatment [25], sensor [26], magnetic optical behavior [27], and biomedical [28]. Besides this, CoFe₂O₄ was also used as photocatalysts for the degradation of organic dyes because of its chemical stability and the narrow bandgap makes it active under visible light. Some of the scientific reports are quoted below which are evident for the photocatalytic activity of the CoFe₂O₄

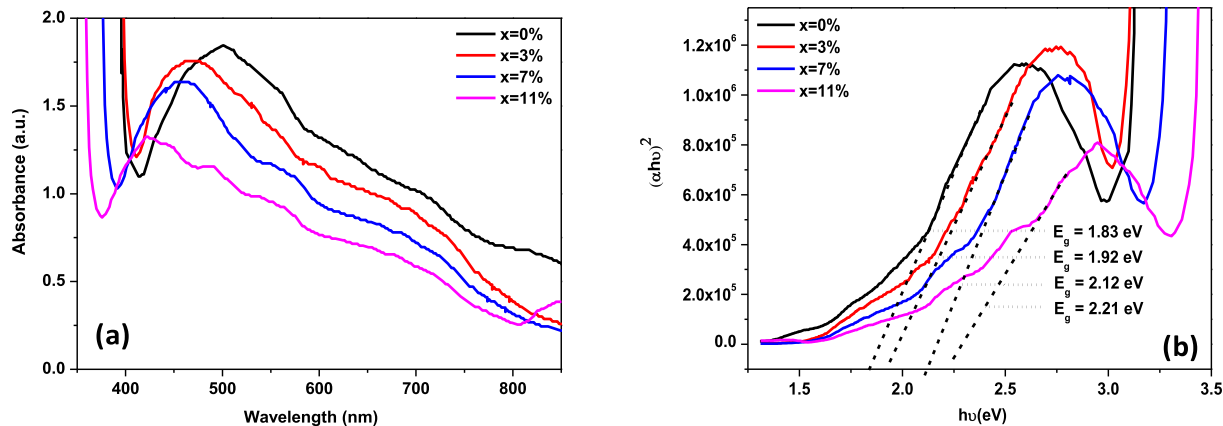


Fig. 2. (a) The UV-Visible absorption spectrum of CoFe₂O₄ and Ni-doped CoFe₂O₄ NPs and (b) The Tauc's plot of CoFe₂O₄ and Ni-doped CoFe₂O₄ NPs.

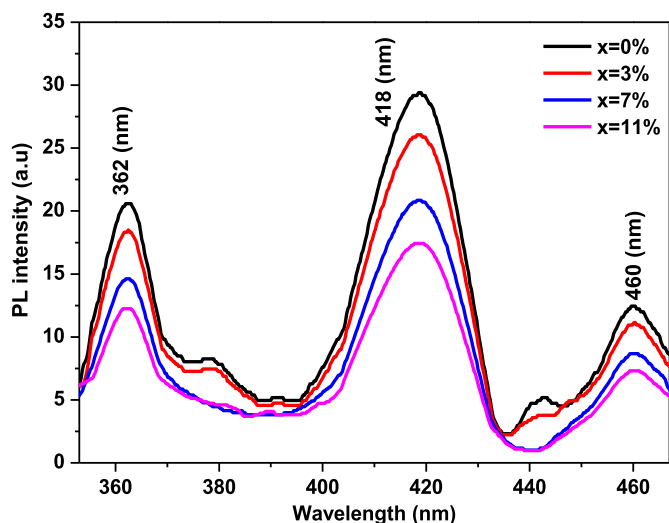


Fig. 3. The PL spectrum of CoFe_2O_4 and Ni-doped CoFe_2O_4 NPs.

nanoparticles (NPs). Zhenlu Li et al. reported the photocatalytic activity of $\text{CoFe}_2\text{O}_4/\text{AgBr}$ among Methyl orange, RhB and MB [29]. Mg-doped CoFe_2O_4 NPs and Zn doped CoFe_2O_4 NPs for degrading RhB dye were reported by M. Sundararajan et al. [30,31]. CoFe_2O_4 NPs degrading Methylene Blue (MB) dye was reported by A. Kalam et al. [32]. L. Gan et al. reported graphene assisted CoFe_2O_4 NPs for degrading MB dye [33].

There are many methods are available for the development of NPs such as microwave-assisted, hydrothermal, combustion route, sol-gel technique, micro-emulsion method, solvothermal, Co-precipitation, etc. Out of these, the Co-precipitation route is the simplest way for synthesizing the NPs. In this work, the Ni-doped CoFe_2O_4 NPs with a different weight percentage of Nickel atoms was developed via a simple Co-precipitation route. The optical, morphological, structural analyses were carried out and the photocatalytic behaviors of as-prepared samples were studied under direct sunlight.

2. Materials and method

The chemicals used to synthesis CoFe_2O_4 and Ni-doped CoFe_2O_4 NPs are Cobalt (II) nitrate hexahydrate ($\text{Co}(\text{NO}_3)_2 \cdot 6\text{H}_2\text{O}$), Ferric (III) nitrate nonahydrate ($\text{Fe}(\text{NO}_3)_3 \cdot 9\text{H}_2\text{O}$), Nickel (II) nitrate hexahydrate ($\text{Ni}(\text{NO}_3)_2 \cdot 6\text{H}_2\text{O}$), sodium hydroxide pellets (NaOH), and double-distilled water. All the chemicals and reagents are from Merck brand with 99.9% purity which is used here without further purification. 0.1 M of cobalt nitrate and 0.2 M of ferric nitrate were dissolved in 100 ml of

distilled water with the use of magnetic stirrer. The solution was kept under constant and vigorous for a few minutes to obtain a homogenous mixture of two salts. After that 4 M of 30 ml, aqueous NaOH solution was added slowly in a drop-wise manner into the above mixture with the help of the burette. After completion of adding the entire reducing agent into the solution, the mixture was kept undisturbed at constant stirring for 6hr. Then the stirrer is stopped and the beaker containing solution is kept undisturbed for a whole night allows the particles to completely settle at the bottom of the beaker. The precipitate is then centrifuged at 3000 rpm and washed with ethanol for further purification. Then the particle is dried in a hot air oven at 80°C . Further, the particle is annealed at 400°C for 2hr. The above procedure is repeated for the preparation of Ni-doped CoFe_2O_4 NPs by simply adding Nickel nitrate to the solution at different wt% and the corresponding wt% is reduced from Cobalt nitrate.

3. Photocatalytic test

The photocatalytic activity of the as-prepared samples was examined with three different organic dyes namely Methylene Blue (MB), Rhodamine B (RhB) and Crystal Violet (CV) are used as a water pollutant. For the analysis 100 ml of 5 mg/L dye solution, 0.1 mg of the sample, and 2 ml of hydrogen peroxide (H_2O_2) 30% solution were used. All the dyes were taken in separate beakers and all these experiments were done under direct sunlight.

4. Results and discussion

4.1. structural analysis

The Powder X-ray diffraction analysis is used to study the crystalline nature, crystal structure, lattice parameters, and also the phases of polycrystalline materials. Fig. 1a shows the XRD pattern of the as-prepared samples named as $\text{Ni}_x\text{Co}_{(100-x)}\text{Fe}_2\text{O}_4$ ($x = 3$ wt%, 7 wt%, 11 wt%). The peaks observed respected to the planes (2 2 0), (3 1 1), (4 0 0), (4 4 0) and (5 1 1) for corresponding 2θ values confirms that the prepared sample has a spinel-type FCC structure belongs to the space group $Fd\bar{3}m$. Further, the pattern is well-matched with the (JCPDS No. 22-1012) indicates the CoFe_2O_4 phase of as-prepared samples. The lattice parameter of the samples was calculated using the formula

$$a = d\sqrt{h^2 + k^2 + l^2} \quad (1)$$

It is noticed that the lattice parameter is decreasing with increasing the content of nickel ions. This is due to the smaller ionic radius nickel ions (0.63 \AA) is replacing the cobalt ion (0.78 \AA) site [34]. The peak position is also slightly shifted towards the lower angle side with increasing nickel content and is shown in Fig. 1b [35]. The graph showing the variation of the lattice parameter with respect to Ni^{2+}

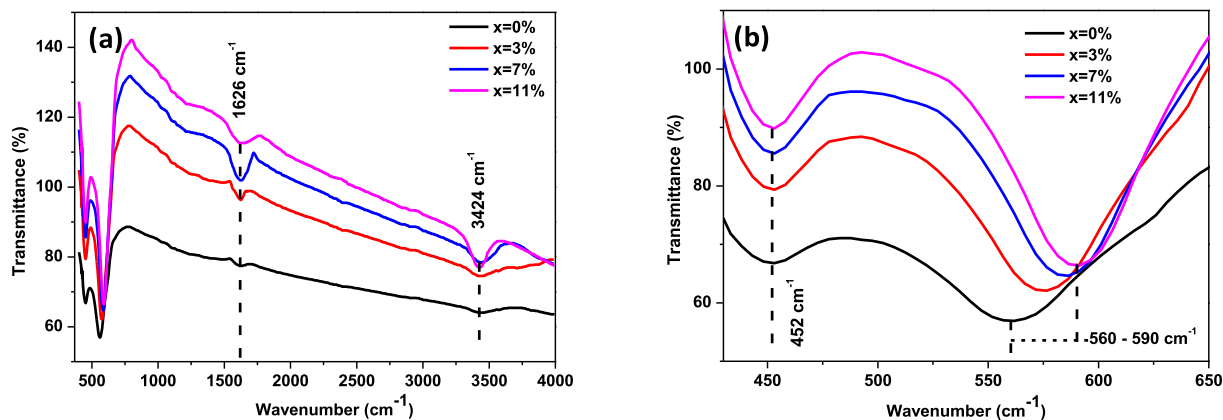


Fig. 4. (a & b) The FT-IR spectrum of CoFe_2O_4 and Ni-doped CoFe_2O_4 NPs.

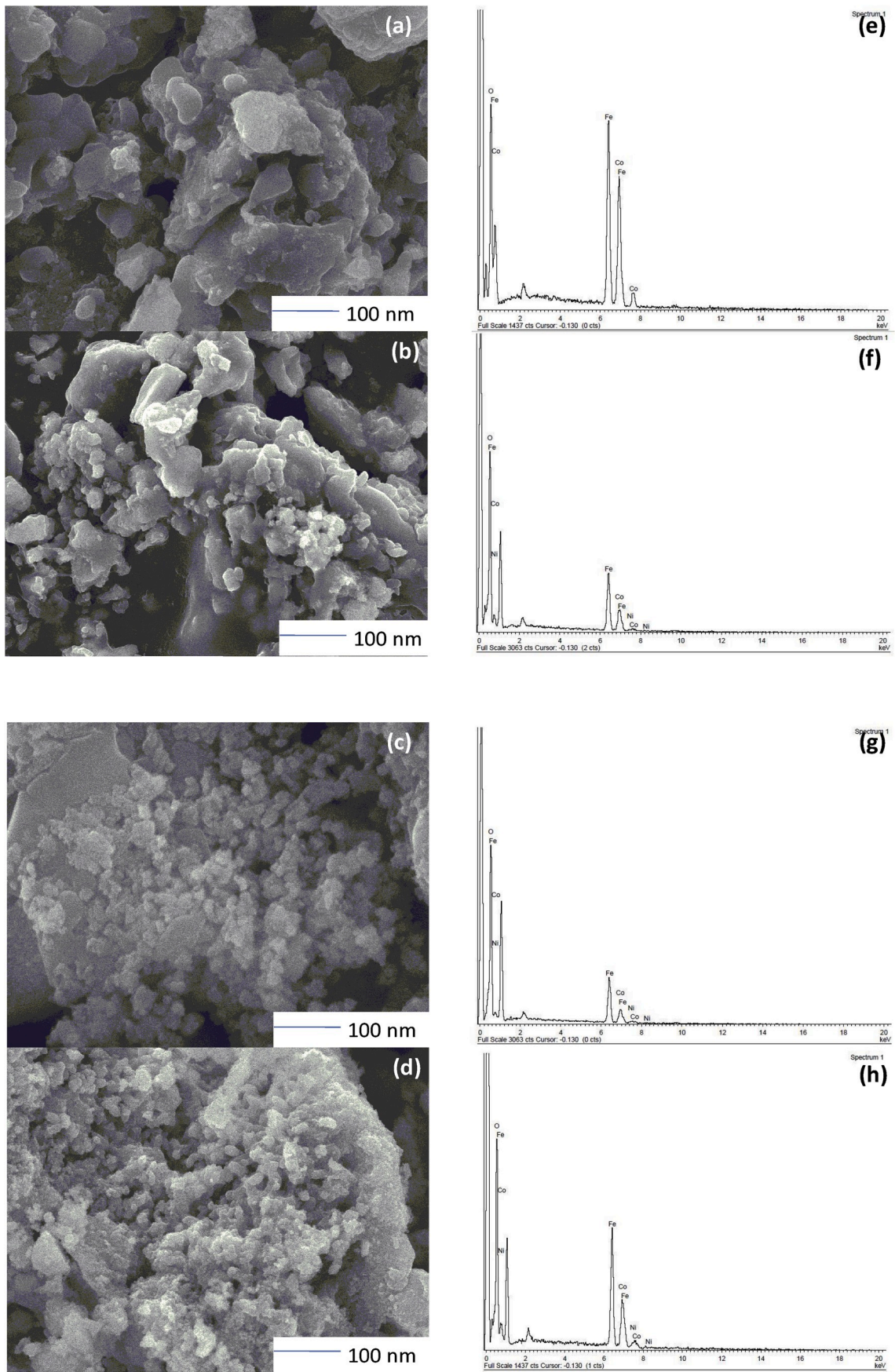


Fig. 5. (a, b, c, & d) SEM images of CoFe₂O₄ and Ni-doped CoFe₂O₄ NPs and (e, f, g & h) The EDAX spectrum of CoFe₂O₄ and Ni-doped CoFe₂O₄ NPs.

Table 2
Elemental comparison table of CoFe_2O_4 and Ni-doped CoFe_2O_4 NPs.

Samples	O (wt %)	Fe (wt %)	Co (wt %)	Ni (wt %)
CoFe_2O_4	27.46	40.10	32.44	0
$\text{Ni}_{3\%}\text{Co}_{(100-3\%)}\text{Fe}_2\text{O}_4$	37.75	40.25	20.42	1.58
$\text{Ni}_{7\%}\text{Co}_{(100-7\%)}\text{Fe}_2\text{O}_4$	41.48	37.26	18.63	2.63
$\text{Ni}_{11\%}\text{Co}_{(100-11\%)}\text{Fe}_2\text{O}_4$	38.61	40.33	16.59	4.47

content is in Fig. 1c and the lattice parameters, as well as the predominant peak positions, were tabulated in Table 1. The broadening of the peak shows the low crystalline nature of the material due to agglomeration during precipitation and also by low annealing temperature. The average particle size was calculated by the classical method i.e. using Scherrer formula.

$$D = \frac{K\lambda}{\beta \cos\theta} \quad (2)$$

Here (D) is the particle size, K, λ , β , θ are the shape factor, X-ray wavelength, FWHM, and diffraction angle respectively. The particle size is found to be 40.23 nm, 41.56 nm, 42.38 nm, and 43.15 nm for pure cobalt ferrite, 3 wt% Ni, 7 wt% Ni, and 11 wt% Ni-doped samples respectively.

4.2. optical studies

(a) UV-Visible spectroscopy

The UV-Visible spectroscopy is used to analyze the optical behavior like absorbance, reflectance, and transmittance of the synthesized materials. The optical bandgap of the material was also calculated from the UV data using Tauc's relation.

$$\alpha h\nu = A(h\nu - E_g)^{1/2} \quad (3)$$

where A, E_g , α , h, and ν are the proportionality constant, bandgap, absorption coefficient, Planck's constant, and light frequency respectively.

The UV absorbance spectrum of the as-prepared samples was shown in Fig. 2a and the corresponding Tauc plot graph is shown in Fig. 2b from which the bandgap is estimated. From the absorbance spectrum the blue shift is observed with increasing nickel content this leads to an increase in the bandgap of the material. The increase in bandgap i.e. the blue shift occurs with the increase in Ni^{2+} ions is due to the quantum confinement effect [36,37]. The bandgap value is found to be 1.83 eV, 1.92 eV, 2.12 eV, and 2.21 eV for pure cobalt ferrite, 3 wt% Ni, 7 wt% Ni, and 11 wt% Ni-doped samples respectively. The observed bandgap values are closely matched with the research article reported by C. Singh et al. [38]. Although there is a slight increase in the bandgap value, the utmost achieved band gap is also within the visible region; hence all the synthesized materials are still active in the visible region of the solar spectrum.

(b) Photoluminescence studies

The PL spectrum was recorded at room temperature to scrutinize the occurrence of electron-hole recombination and to gather the information on defect states [39]. Fig. 3 represents the PL spectrum of the as-prepared samples with the excitation wavelength of 320 nm. The PL emission spectrum arises when the material is subjected to the light photons; electrons in the material are getting excited by the absorption of photons and return to the ground state depending on the surface defect, vacancies, surface oxides, and size. The peak arises at 362 nm in the near band edge emission owing to excitons inherent transition between valence and conduction band [40]. The blue emission peak was

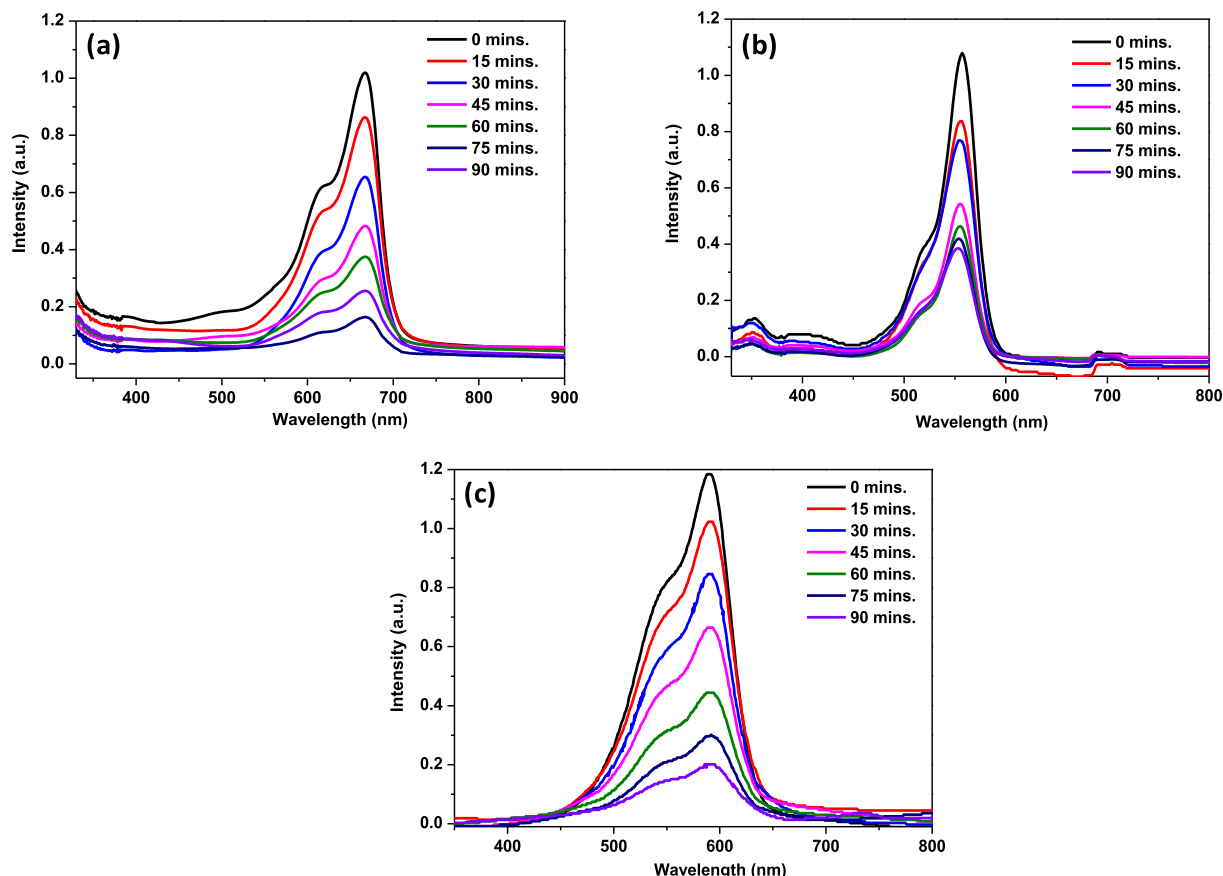


Fig. 6. (a, b & c) Time-dependent UV-Vis absorption spectra for the reduction of MB, RhB and CV dye with catalyst $\text{Ni}_{11\%}\text{Co}_{(100-11\%)}\text{Fe}_2\text{O}_4$.

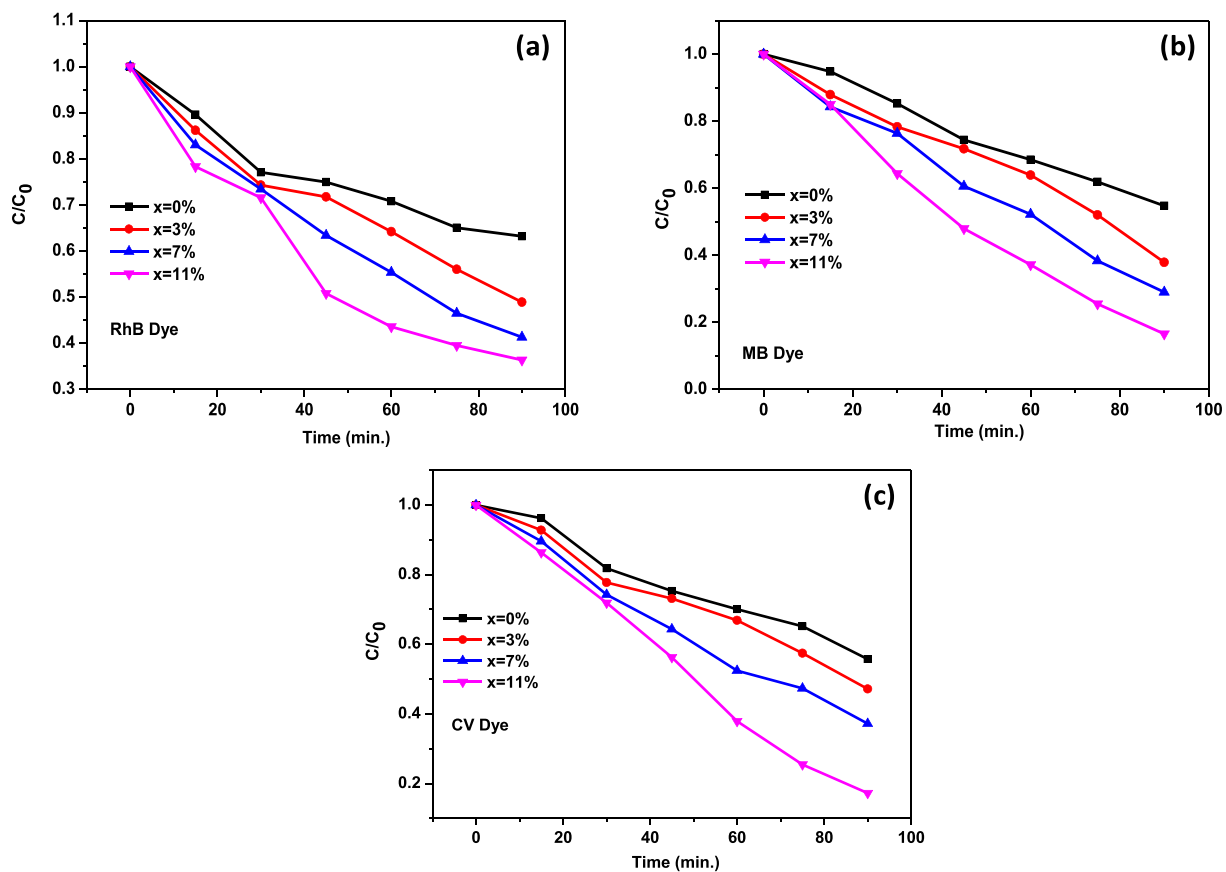


Fig. 7. (a, b & c) Time vs concentration of MB, RhB and CV dye.

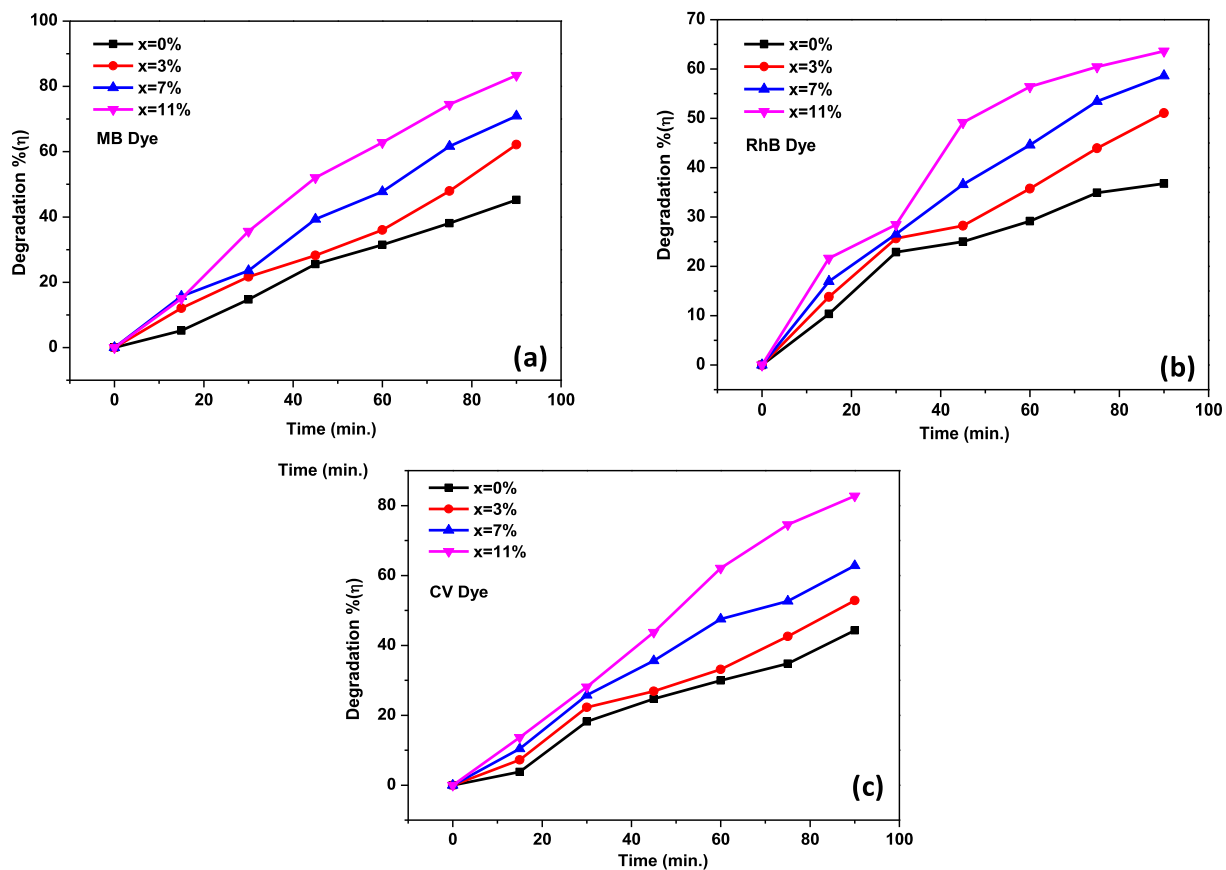


Fig. 8. (a, b & c) Time vs Degradation percentage of MB, RhB and CV dye.

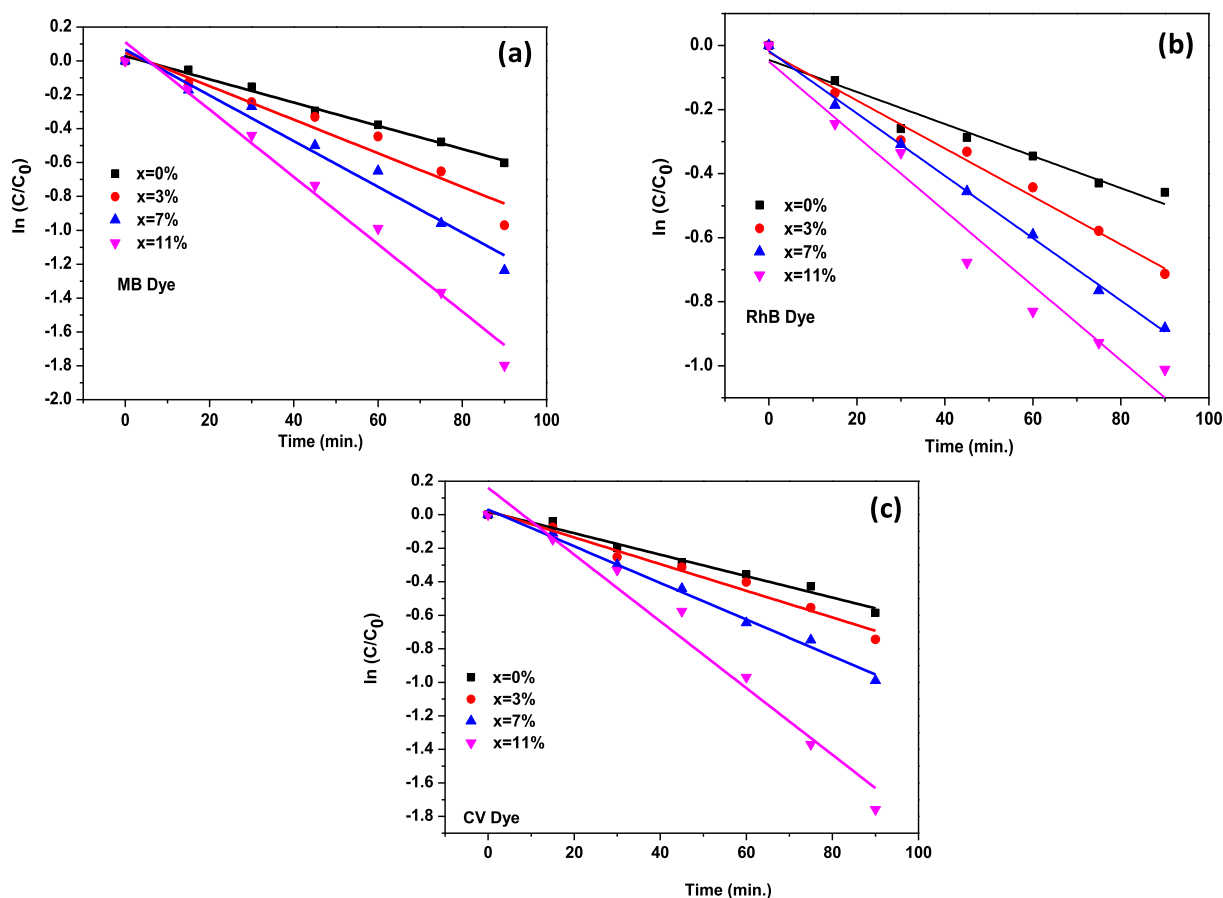


Fig. 9. (a, b & c) Time vs. Rate constant for MB, RhB and CV dye.

observed at the 460 nm is attributed to the Fe^{3+} transition in the ferrite sites [41]. The predominant peak appears at 418 nm is the result of free electrons is intensely trapped at the holes generated by the photons in the oxygen vacancies [42]. It is observed from the PL spectrum that the intensity of every peak gets diminished with the increase in the nickel content, this may due to the increase of band gap which reduces the rate of electron-hole recombination. Hence this result is well agreed with the UV studies.

4.3. FTIR analysis

The FTIR spectrum of the as-prepared samples was recorded in the frequencies ranges from 4000 to 350 cm^{-1} is shown in Fig. 4(a and b). Generally, two peaks were observed due to M – O bond vibrations corresponding to the tetrahedral and octahedral sites in the spinel ferrite sub-lattice [43]. The peak located at $\sim 1626 \text{ cm}^{-1}$ corresponds to the stretching mode vibration of surface adsorbed H–O–H molecules, whereas the peak at $\sim 3424 \text{ cm}^{-1}$ is related to bending vibration mode of H–O–H [44]. The transmittance peak observed from 450 to 385 cm^{-1} is generally related to the M – O stretching vibration at tetrahedral sites and peak at 600–550 cm^{-1} is assigned to the M – O stretching vibration at octahedral sites [45]. From the FTIR spectrum, it is noticed that the peak arises from the tetrahedral site is shifted towards the higher frequency side with respect to the increase in nickel wt %. This phenomenon occurred due to the occupancy of Ni^{2+} ions in the octahedral sites and forces the Fe^{3+} ions to the tetrahedral sites so that the Fe ions with lower atomic mass is replacing the Co ions position at the tetrahedral sites [46]. These FTIR analyses confirm that the synthesized samples are spinel ferrites and get agree with the XRD analysis.

4.4. morphological and elemental analysis

The SEM images of all samples were displayed in Fig. 5 (a, b, c, & d). The particles get agglomerates and show irregularity is maybe due to the less crystalline nature of the material which was already discussed in

Table 3

Dye degradation analysis comparison table of CoFe_2O_4 and Ni-doped CoFe_2O_4 NPs.

Dye	Samples	Rate constant (k) (s^{-1})	(R^2) value	Degradation %
Methylene Blue	CoFe_2O_4	6.86×10^{-3}	0.99069	45.21
	$\text{Ni}_{3\%}\text{Co}_{(100-3\%)}\text{Fe}_2\text{O}_4$	9.92×10^{-3}	0.93513	62.16
	$\text{Ni}_{7\%}\text{Co}_{(100-7\%)}\text{Fe}_2\text{O}_4$	13.49×10^{-3}	0.97043	70.97
	$\text{Ni}_{11\%}\text{Co}_{(100-11\%)}\text{Fe}_2\text{O}_4$	19.88×10^{-3}	0.98088	83.41
Rhodamine B	CoFe_2O_4	5.00×10^{-3}	0.9416	36.78
	$\text{Ni}_{3\%}\text{Co}_{(100-3\%)}\text{Fe}_2\text{O}_4$	7.49×10^{-3}	0.98307	51.07
	$\text{Ni}_{7\%}\text{Co}_{(100-7\%)}\text{Fe}_2\text{O}_4$	9.74×10^{-3}	0.99732	58.64
	$\text{Ni}_{11\%}\text{Co}_{(100-11\%)}\text{Fe}_2\text{O}_4$	11.6×10^{-3}	0.95698	63.62
Crystal Violet	CoFe_2O_4	6.4×10^{-3}	0.97822	44.28
	$\text{Ni}_{3\%}\text{Co}_{(100-3\%)}\text{Fe}_2\text{O}_4$	7.9×10^{-3}	0.97496	52.84
	$\text{Ni}_{7\%}\text{Co}_{(100-7\%)}\text{Fe}_2\text{O}_4$	10.93×10^{-3}	0.99167	62.79
	$\text{Ni}_{11\%}\text{Co}_{(100-11\%)}\text{Fe}_2\text{O}_4$	19.9×10^{-3}	0.96066	82.76

Table 4
Comparison table of previously reported work with present work for dye degradation analysis.

S.NO.	Materials Used	Dyes Used	Efficiency (%) η	Irradiation Source and Time		Reference
1.	CoFe ₂ O ₄ – ZnO (Hydrothermal route)	Methylene Blue	78	60 (min.)	UV- Irradiation/	[48]
2.	CoFe ₂ O ₄ – ZnO (Colloidal route)	Methyl Orange	93.9	5 (hr.)	UV- Irradiation/	[49]
3.	CoFe ₂ O ₄ /BiVO ₄ (Hydrothermal route)	Methylene Blue	72.47	240 (min.)	Halogen lamp (Visible light source)/	[50]
4.	CoFe ₂ O ₄ : Mg (Microwave combustion route)	Rhodamine B	99	255 (min.)	Halogen lamp (Visible light source)/	30
5.	CoFe ₂ O ₄ : Zn (Microwave combustion route)	Rhodamine B	99	210(min.)	Tungsten halide lamp (UV-Visible light source)/	31
6.	CoFe ₂ O ₄ (Modified solvothermal synthesis)	Methylene Blue	80	140 (min.)	Tungsten halide lamp (UV-Visible light source)/	32
7.	CoFe ₂ O ₄ : Ni (Co-precipitation route)	Methylene Blue	83.41	90 (min.)	Sunlight	Present Work
		Rhodamine B	63.62			
		Crystal Violet	82.76			

XRD analysis. From the images, it is observed that all the samples have a porous nature and this porosity plays a vital role in the photocatalytic activity. The elemental compositions of the prepared sample were studied with the help of EDAX instrumentation is shown in Fig. 5 (e, f, g & h) the weight percentage of the as-prepared samples was tabulated in Table 2.

5. The photocatalytic performance of CoFe₂O₄ and Ni-doped CoFe₂O₄

The Photocatalytic performance of as-prepared samples was examined among three organic dyes namely MB, RhB, and CV. The degradation of dyes with respect to time is recorded using a UV-Vis spectrophotometer. Generally, the degradation of dyes takes place due to the formation of active radicals (O_2^- , $O_2^{\cdot-}$, HOO^{\cdot}/OH^{\cdot}) during the photocatalytic reaction. All three dyes were taken separately and kept under direct sunlight for 90 (min). The aliquots of the dye samples are collected at regular time intervals i.e. every 15 min and analyzed with a UV spectrometer. The maximum degradation efficiency was achieved for 11 wt% Ni-doped CoFe₂O₄ sample as compared to other samples and the UV spectrum of MB, RhB and CV dyes are shown in Fig. 6(a and b, c). The degradation efficiency and decrease in the concentration of dyestuffs with respect time for all samples were calculated and represented in Figs. 7 and 8. It is observed that the degradation efficiency is increased with an increase in nickel wt%. The reason behind this is the cobalt ions which are catalytically less active are replaced by Ni²⁺ ions at the octahedral site and hence the catalytic activity is increased. Moreover, the larger the bandgap will reduce the rate of electron-hole recombination, and this is already discussed in the optical studies [47]. All these photocatalytic studies were examined in two aspects one without H₂O₂ and others with H₂O₂. It is observed that there is no change in the initial concentration of all three dyes when bare samples are incorporated. This is because there is a lack of OH radicals formation due to the faster rate of e^-/h^+ recombination. Hence the H₂O₂ in incorporated in the reaction which acts as a scavenger for photo-generated free electrons produced by the catalyst i.e. as-prepared NPs. This phenomenon will decrease the recombination rate and thus the holes got enough time to react with water molecules to generate OH radicals, on the other hand, H₂O₂ also produces OH radicals due to the acceptance of free electrons. Hence the sufficient formation of OH radicals will increase the degradation efficiency. The rate constant of the reaction was calculated using the below-given formula and the graph is shown in Fig. 9.

$$\ln(C/C_0) = kt \quad (4)$$

Eq. (4) is known as pseudo-first-order kinetics. Here C, C₀ is the initial and final concentration of the dye solution and k is the rate constant with respect to degradation time. The percentage of degradation, rate constant and estimated R² values for all the dyes and samples are tabulated in Table 3. Some of the previously reported cobalt ferrite based metal oxide nanoparticles for as a photocatalyst application is shown in Table 4. The synthesis route is very simple and cost-effective and the photo source for degrading the dye is sunlight; hence there is

no need for any special experimental setup and it is cost-effective because the sunlight is the everlasting source. In addition the degradation efficiency is also higher than that of the previously reported work.

6. Conclusion

The cobalt ferrite and nickel doped cobalt ferrites are successfully synthesized via chemical co-precipitation method. The nature and crystalline size of the NPs were studied by PXRD. The optical behavior of as-prepared samples was analyzed. Furthermore, towards application prospect, all the synthesized samples were separately examined for photocatalytic activity and their overall performance was comparatively discussed. From the results, it is clear that the incorporation of Ni²⁺ ions into the Cobalt lattice will increase the photocatalytic activity of the Cobalt ferrites. Among the three dyes used MB is highly degraded, the second-highest degradation was observed in the CV dye. The as-prepared particle shows less degradation efficiency for RhB dye, this may be due to the molecular structure of the dye. Moreover, the photocatalytic activity of Nickel doped Cobalt ferrites under direct sunlight for the degradation of organic dyestuffs is proved from the above results and thus it can act as an efficient remedy of environmental water pollution.

References

- [1] Y. I Matatov-Meytal, M. Sheintuch, Catalytic abatement of water pollutants, *Ind. Eng. Chem. Res.* 37 (2) (1998) 309–326.
- [2] J.R. Chiou, B.H. Lai, K.C. Hsu, D.H. Chen, One-pot green synthesis of silver/iron oxide composite nanoparticles for 4-nitrophenol reduction, *J. Hazard Mater.* 248 (2013) 394–400.
- [3] L. Liu, G. Zhang, L. Wang, T. Huang, L. Qin, Highly active S-modified ZnFe₂O₄ heterogeneous catalyst and its photo-Fenton behavior under UV-visible irradiation, *Ind. Eng. Chem. Res.* 50 (12) (2011) 7219–7227.
- [4] R. Bauer, G. Waldner, H. Fallmann, S. Hager, M. Klare, T. Krutzler, P. Maletzky, The photo-fenton reaction and the TiO₂/UV process for waste water treatment—novel developments, *Catal. Today* 53 (1) (1999) 131–144.
- [5] A. Houas, H. Lachheb, M. Ksibi, E. Elaloui, C. Guillard, J.M. Herrmann, Photocatalytic degradation pathway of methylene blue in water, *Appl. Catal. B Environ.* 31 (2) (2001) 145–157.
- [6] J. Herney-Ramirez, M.A. Vicente, L.M. Madeira, Heterogeneous photo-Fenton oxidation with pillared clay-based catalysts for wastewater treatment: a review, *Appl. Catal. B Environ.* 98 (1–2) (2010) 10–26.
- [7] A. Gajović, A.M. Silva, R.A. Segundo, S. Sturm, B. Jančar, M. Čeh, Tailoring the phase composition and morphology of Bi-doped goethite-hematite nanostructures and their catalytic activity in the degradation of an actual pesticide using a photo-Fenton-like process, *Appl. Catal. B Environ.* 103 (3–4) (2011) 351–361.
- [8] L. Xue, B. Lu, Z.S. Wu, C. Ge, P. Wang, R. Zhang, X.D. Zhang, Synthesis of mesoporous hexagonal boron nitride fibers with high surface area for efficient removal of organic pollutants, *Chem. Eng. J.* 243 (2014) 494–499.
- [9] J. Xie, W. Meng, D. Wu, Z. Zhang, H. Kong, Removal of organic pollutants by surfactant modified zeolite: comparison between ionizable phenolic compounds and non-ionizable organic compounds, *J. Hazard Mater.* 231 (2012) 57–63.
- [10] N. Pradhan, A. Pal, T. Pal, Silver nanoparticle catalyzed reduction of aromatic nitro compounds, *Colloid. Surface. Physicochem. Eng. Aspect.* 196 (2–3) (2002) 247–257.
- [11] L. Ai, J. Jiang, Catalytic reduction of 4-nitrophenol by silver nanoparticles stabilized on environmentally benign macroscopic biopolymer hydrogel, *Bioresour. Technol.* 132 (2013) 374–377.
- [12] Y.C. Chang, D.H. Chen, Catalytic reduction of 4-nitrophenol by magnetically recoverable Au nanocatalyst, *J. Hazard Mater.* 165 (1–3) (2009) 664–669.
- [13] H. Koga, T. Kitaoka, One-step synthesis of gold nanocatalysts on a micro structured paper matrix for the reduction of 4-nitrophenol, *Chem. Eng. J.* 168 (1) (2011) 420–425.

- [14] W. Zhang, F. Tan, W. Wang, X. Qiu, X. Qiao, J. Chen, Facile, template-free synthesis of silver nanodendrites with high catalytic activity for the reduction of p-nitrophenol, *J. Hazard Mater.* 217 (2012) 36–42.
- [15] J. Feng, L. Su, Y. Ma, C. Ren, Q. Guo, X. Chen, CuFe₂O₄ magnetic nanoparticles: a simple and efficient catalyst for the reduction of nitro phenol, *Chem. Eng. J.* 221 (2013) 16–24.
- [16] P. Yang, A.D. Xu, J. Xia, J. He, H.L. Xing, X.M. Zhang, N.N. Wang, Facile synthesis of highly catalytic activity Ni–Co–Pd–P composite for reduction of the p-Nitrophenol, *Appl. Catal. Gen.* 470 (2014) 89–96.
- [17] V.K. Gupta, N. Atar, M.L. Yola, Z. Üstündağ, L. Uzun, A novel magnetic Fe@ Au core–shell nanoparticles anchored graphene oxide recyclable nanocatalyst for the reduction of nitrophenol compounds, *Water Res.* 48 (2014) 210–217.
- [18] Y.C. Chang, D.H. Chen, Catalytic reduction of 4-nitrophenol by magnetically recoverable Au nanocatalyst, *J. Hazard Mater.* 165 (1–3) (2009) 664–669.
- [19] A.I. Borhan, P. Samoila, V. Hulea, A.R. Jordan, M.N. Palamaru, Effect of Al³⁺ substituted zinc ferrite on photocatalytic degradation of Orange I azo dye, *J. Photochem. Photobiol. Chem.* 279 (2014) 17–23.
- [20] M. Rahimi-Nasrabadi, M. Behpour, A. Sobhani-Nasab, M.R. Jeddy, Nanocrystalline Ce-doped copper ferrite: synthesis, characterization, and its photocatalyst application, *J. Mater. Sci. Mater. Electron.* 27 (11) (2016) 11691–11697.
- [21] R. Sharma, S. Singhal, Photodegradation of textile dye using magnetically recyclable heterogeneous spinel ferrites, *J. Chem. Technol. Biotechnol.* 90 (5) (2015) 955–962.
- [22] S.K. Jesudoss, J.J. Vijaya, L.J. Kennedy, P.I. Rajan, H.A. Al-Lohedan, R. J. Ramalingam, M. Bououdina, Studies on the efficient dual performance of Mn_{1-x}Ni_xFe₂O₄ spinel nanoparticles in photodegradation and antibacterial activity, *J. Photochem. Photobiol. B Biol.* 165 (2016) 121–132.
- [23] A. Samavati, A.F. Ismail, Antibacterial properties of copper-substituted cobalt ferrite nanoparticles synthesized by co-precipitation method, *Particuology* 30 (2017) 158.
- [24] J. Ahmed, S.M. Alshehri, A.N. Alhabarah, T. Ahmad, Nitrogen doped cobalt ferrite/carbon (NCFC) nanocomposites for supercapacitor application, *Chem Electro Chem* 4 (2017) 2952.
- [25] D.H. Kim, D.E. Nikles, D.T. Jhonson, C.S. Brazel, Heat generation of aqueously dispersed CoFe₂O₄ nanoparticles as heating agents for magnetically activated drug delivery and hyperthermia, *J. Magn. Magn Mater.* 320 (2008) 2390.
- [26] J.A. Paulsen, A. P Ring, C.C.H. Lo, J.E. Snyder, D.C. Jiles, Manganese substituted cobalt ferrite magnetostrictive materials for magnetic stress sensor applications, *J. Appl. Phys.* 97 (2005), 044502.
- [27] D. Erdem, N.S. Bingham, F.J. Heiligtag, N. Pilet, P. Warnicke, L.J. Heyderman, M. Niederberger, CoFe₂O₄ and CoFe₂O₄-SiO₂ nanoparticle thin films with perpendicular magnetic anisotropy for magnetic and magneto-optical applications, *Adv. Funct. Mater.* 26 (2016) 1954.
- [28] M.P. Pileni, Magnetic fluids: fabrication, magnetic properties and organization of nanocrystals, *Adv. Funct. Mater.* 11 (2001) 323.
- [29] Z. Li, J. Ai, M. Ge, A facile approach assembled magnetic CoFe₂O₄/AgBr composite for dye degradation under visible light, *Journal of Environmental Chemical Engineering* 5 (2017) 1394–1403.
- [30] M. Sundararajan, L.J. Kennedy, P. Nithya, J.J. Vijaya, M. Bououdina, Visible light driven photocatalytic degradation of rhodamine B using Mg doped cobalt ferrite spinel nanoparticles synthesized by microwave combustion method, *J. Phys. Chem. Solid.* 108 (2017) 61–75.
- [31] M. Sundararajan, V. Sailaja, L.J. Kennedy, J.J. Vijaya, Photocatalytic degradation of rhodamine B under visible light using nanostructured zinc doped cobalt ferrite: kinetics and mechanism, *Ceram. Int.* 43 (1) (2017) 540–548.
- [32] A. Kalam, A.G. Al-Sehemi, M. Assiri, G. Du, T. Ahmad, I. Ahmad, M. Pannipara, Modified solvothermal synthesis of cobalt ferrite (CoFe₂O₄) magnetic nanoparticles photocatalysts for degradation of methylene blue with H₂O₂/visible light, *Results in physics* 8 (2018) 1046–1053.
- [33] L. Gan, S. Shang, C.W.M. Yuen, S.X. Jiang, E. Hu, Hydrothermal synthesis of magnetic CoFe₂O₄/graphene nanocomposites with improved photocatalytic activity, *Appl. Surf. Sci.* 351 (2015) 140–147.
- [34] A. Kumar, N. Yadav, D.S. Rana, P. Kumar, M. Arora, R.P. Pant, Structural and magnetic studies of the nickel doped CoFe₂O₄ ferrite nanoparticles synthesized by the chemical co-precipitation method, *J. Magn. Magn Mater.* 394 (2015) 379–384.
- [35] A.M. El Sayed, “Influence of zinc content on some properties of Ni–Zn ferrites”, *Ceram. Int.* 28 (2002) 363–367.
- [36] S.S. Nair, M. Mathews, M.R. Anantharaman, Evidence for blueshift by weak exciton confinement and tuning of bandgap in superparamagnetic nanocomposites, *Chem. Phys. Lett.* 406 (4–6) (2005) 398–403.
- [37] S. Chakrabarty, A. Dutta, M. Pal, Effect of Mn and Ni codoping on ion dynamics of nanocrystalline cobalt ferrite: a structure property correlation study, *Electrochim. Acta* 184 (2015) 70–79.
- [38] C. Singh, A. Goyal, S. Singhal, Nickel-doped cobalt ferrite nanoparticles: efficient catalysts for the reduction of nitroaromatic compounds and photo-oxidative degradation of toxic dyes, *Nanoscale* 6 (14) (2014) 7959–7970.
- [39] R. Bhargava, P.K. Sharma, R.K. Dutta, S. Kumar, A.C. Pandey, N. Kumar, Influence of Co-doping on the thermal, structural, and optical properties of sol–gel derived ZnO nanoparticles, *Mater. Chem. Phys.* 120 (2–3) (2010) 393–398.
- [40] A. Ray, M. Roy, J. Ghosh, A. Ramos-Ramón, S. Saha, U. Pal, S.K. Bhattacharya, S. Das, Study on charge storage mechanism in working electrodes fabricated by sol-gel derived spinel NiMn₂O₄ nanoparticles for supercapacitor application, *Appl. Surf. Sci.* 463 (2019) 513–525.
- [41] B.J. Rani, M. Ravina, B. Saravanakumar, G. Ravi, V. Ganesh, S. Ravichandran, R. Yuvakkumar, Ferrimagnetism in cobalt ferrite (CoFe₂O₄) nanoparticles, *Nano-Structures & Nano-Objects* 14 (2018) 84–91.
- [42] A. Manikandan, M. Durka, K. Seevakan, S. Antony, A novel one-pot combustion synthesis and opto-magnetic properties of magnetically separable spinel MnMgFeO (0.0 ≤ x ≤ 0.5) nanophotocatalysts, *J. Supercond. Nov. Magnetism* 28 (4) (2015).
- [43] R.D. Waldron, Infrared spectra of ferrites, *Phys. Rev.* 99 (6) (1955) 1727.
- [44] W.B. Carpenter, J.A. Fournier, R. Biswas, G.A. Voth, A. Tokmakoff, Delocalization and stretch-bend mixing of the HOH bend in liquid water, *J. Chem. Phys.* 147 (8) (2017), 084503.45.
- [45] B.P. Jacob, A. Kumar, R.P. Pant, S. Singh, E.M. Mohammed, Influence of preparation method on structural and magnetic properties of nickel ferrite nanoparticles, *Bull. Mater. Sci.* 34 (7) (2011) 1345–1350.
- [46] Q.M. Wei, J.B. Li, Y.J. Chen, Cation distribution and infrared properties of Ni_xMn_{1-x}Fe₂O₄ ferrites, *J. Mater. Sci.* 36 (21) (2001) 5115–5118.
- [47] E. Casbeer, V.K. Sharma, X.Z. Li, Synthesis and photocatalytic activity of ferrites under visible light: a review, *Separ. Purif. Technol.* 87 (2012) 1–14.
- [48] G. Zhang, W. Xu, Z. Li, W. Hu, Y. Wang, Preparation and characterization of multi-functional CoFe₂O₄-ZnO nanocomposites, *J. Magn. Magn Mater.* 321 (2009) 1424–1427.
- [49] A. Wilson, S.R. Mishra, R. Gupta, K. Ghosh, Preparation and photocatalytic properties of hybrid core–shell reusable CoFe₂O₄-ZnO nano spheres, *J. Magn. Magn Mater.* 324 (2012) 2597–2601.
- [50] S. Duangjam, K. Wetchakun, S. Phanichphant, N. Wetchakun, Hydrothermal synthesis of novel CoFe₂O₄/BiVO₄ nanocomposites with enhanced visible-light-driven photocatalytic activities, *Mater. Lett.* 181 (2016) 86–91.